J. Fluid Mech. (1977), *vol.* 79, *part* 4, *pp.* 715–743
Printed in Great Britain

On the evolution of the system of wind drift currents and Langmuir circulations in the ocean. Part 1. Theory and averaged current

By S. LEIBOVICH

Sibley School of Mechanical and Aerospace Engineering,
Cornell University, Ithaca, New York 14853

(Received 9 February 1976)

A theory for the evolution of the wind drift current and of the Langmuir circulations in infinitely deep water of constant density is presented. The model improves and extends a recent quasi-steady theory of Craik & Leibovich which asserts that the Langmuir circulations arise from a nonlinear interaction between surface waves and the frictional wind drift current. In turn, the development of the wind drift should be strongly influenced by Langmuir circulations, when they are present, and the two current systems are therefore treated here as a single inseparable system driven by a prescribed wind stress and surface wave field. Mixing by the vertical motions in the Langmuir circulations is shown to yield solutions for the wind drift, obtained both analytically and numerically, which are consistent with experiments and with field observations. The model yields a streaky flow pattern with a mean motion much like a turbulent wall layer, although the model is deterministic. In particular, it is found that a 'viscous sublayer' joins surface water to a logarithmic 'inertial sublayer' below. The scaling rules that emerge from the theory allow the surface speed of the wind drift to reach nearly full development in a matter of minutes.

1. Introduction

The application of a wind stress to the surface of a lake or ocean gives rise to a drift current in a thin layer near the surface. Part of the drift arises from a second-order streaming due to the wave motion that is concurrently created, but, at least for short fetches (Wu 1975), the major part of the drift is due to direct momentum transfer from the wind to the water mass. The wind stress is communicated to the larger body of water below by tractions transmitted across this 'wind-driven drift current'. The importance of this thin layer to dynamical processes of the air–sea interface, and to the fate of pollutants introduced at the surface, has been emphasized by Wu (1969, 1975).

Observations of the wind drift current in lakes (Bye 1965) and in laboratory experiments (Wu 1975; Shemdin 1972) indicate that the mean drift current defect (the difference between the surface and local values of the mean current) closely resembles the flow in a turbulent wall-bounded shear flow. In particular, a very

thin viscous sublayer (Wu 1975) connects the surface to a logarithmic friction law (Wu 1975; Bye 1965; Shemdin 1972).

A different set of observations has been made that suggests another similarity between turbulent wall boundary layers and the upper layers of the wind-driven sea. Both display a surprisingly coherent feature of streaks oriented in the streamwise direction. When the wind drift is observed relative to its average surface value, the streaks contain slowly moving fluid; analogous behaviour to this has been reported in the turbulent wall boundary layer (cf. Kline *et al.* 1967). In the ocean, these streaks have been attributed to subsurface vortex motions known as Langmuir circulations (see Craik & Leibovich (1976) or Faller (1971) for references), although the connexion has been disputed at times in the past.

The importance of the Langmuir circulations, when they exist, to the vertical transfer of momentum to the water below was brought out by Gordon (1970); it was also stressed by Leibovich & Ulrich (1972) and re-emphasized by Craik & Leibovich (1976). A method for analysing the Langmuir circulations was developed by Craik & Leibovich; it allowed the circulations to be comparable in magnitude with the wind-directed currents. In their formulation, the Langmuir circulations and the wind drift current were treated as components of a single interdependent current system. This is in accordance with observations which show (Scott *et al.* 1969) that the maximum vertical speeds in the Langmuir circulations are of the same order ($\frac{1}{4}$–$\frac{1}{3}$ as large) as the surface drift speeds (including the wave drift). Craik & Leibovich (1976) concentrated on the quasi-steady Langmuir circulations and did not attempt to calculate the wind drift current. (Instead, the wind drift was assumed to the logarithmic profile reported by Bye 1965.)

In this paper, the focus is on the mean wind drift current. The theory of Craik & Leibovich is extended to allow calculation of the evolution of the wind drift from a state of rest in an ocean of infinite depth and constant density. There is no steady state for the problem in the (assumed) absence of Coriolis accelerations, and the total momentum imparted to the water by a constant wind stress grows linearly with time in proportion to the applied stress.

The nature of the theory and the results obtained may be sumarized as follows: The instability of the air–water interface under an applied wind stress gives rise to water waves with a directional spectrum symmetric about the wind. The theory does not consider the growth phase of the wave motion, which is assumed to be given and invariant with time. Under circumstances detailed by Craik & Leibovich (1976), a surface wave field with directional propagation characteristics that are symmetric with respect to the wind direction can produce a wave drift which is independent of the wind direction and of time and which is periodic in the cross-wind direction. Although the wave drift usually rises in a Langrangian context, here it emerges in a purely Eulerian framework. The wave drift rotates and stretches vortex lines and results in a production of streamwise vorticity, and the consequent mixing enhances the development of the wind drift current. A conceptual sketch is given in figure 1.

Under assumptions explained in the paper, a theory that includes all of these effects is developed. The result is a set of nonlinear time-dependent equations

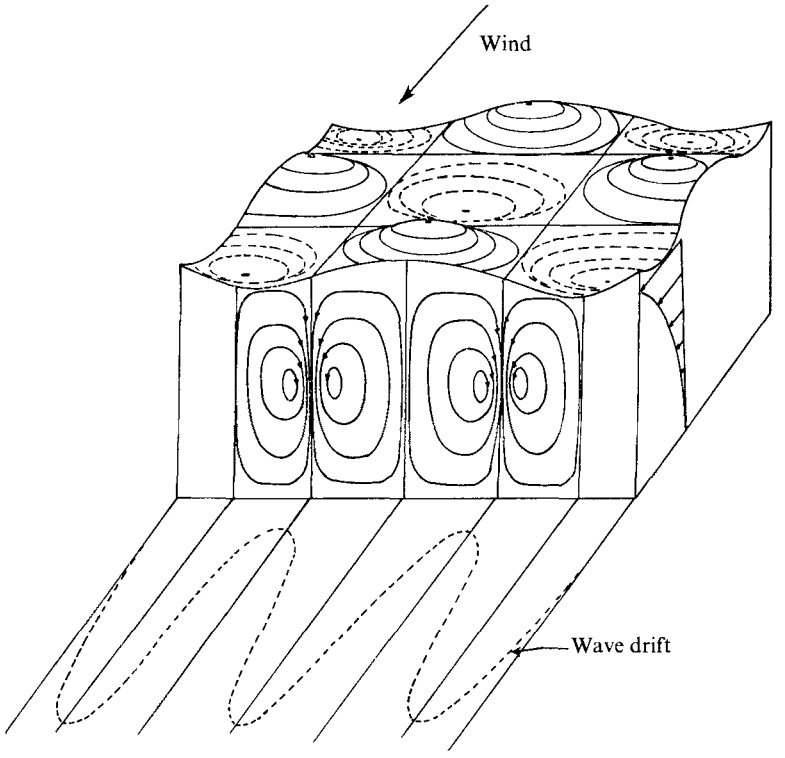

FIGURE 1. A sketch illustrating the concept of the theory. The wave pattern advances in the wind direction, creating a drift that is second order in wave slope. The drift is larger where the excursion of the water from the mean surface is greater, creating the possibility of an undulating wave drift. Vortex lines in the frictional current are distorted producing a streamwise vorticity component and mixing due to the induced vertical motions. This mixing causes a feedback, and alters the frictional current.

bearing a strong resemblance to those governing thermal convection in two space dimensions. These equations are solved analytically for small time, and numerically for arbitrary time. The behaviour of the mean wind drift is then extracted from the complete solution. Here the 'mean' drift refers to an average across the wind of the wind-directed drift profile, which is periodic in the cross-wind direction.

The formulation of the problem in terms of an initial-value problem is much more satisfactory than the earlier work by Craik & Leibovich: the resulting theory is simpler, and the input parameters are more directly related to the physical problem. The final equations are shown to depend upon only two dimensionless parameters. One parameter, which I propose should be called the 'Langmuir number' La, is like an Ekman (or inverse Reynolds) number and the other is an angle θ describing the directional characteristics of the waves. The periodic wind drift in the theory is proportional to $u_*^2/\nu_T\kappa$, where u_* is the water friction velocity determined by the applied wind stress, ν_T is an eddy viscosity due to

turbulent motions on scales smaller than the wavelength of the surface waves, which is $2\pi/\kappa$. The cross-plane velocities are proportional to

$$\frac{\epsilon u_*}{\kappa}\left(\frac{\sigma}{\nu_T}\right)^{\frac{1}{2}},$$

where ϵ is a parameter proportional to the wave slope, and $\sigma = (g\kappa)^{\frac{1}{2}}$ is the wave angular frequency. The motions develop on a time scale with unit T_d given by

$$T_d = \sigma^{-1}(\nu_T\sigma)^{\frac{1}{2}}/\epsilon u_*.$$

By appeal to experimental findings, it is shown in § 7 that the product $\nu_T\kappa$ can be estimated by $k\gamma u_*$, where k is von Kármán's constant and γ is a numerical factor which depends upon the Langmuir number and θ. For two cases calculated in this paper, $\gamma \approx 0{\cdot}1$. When ν_T is eliminated in this way,

$$T_d \sim \sigma^{-1}\epsilon^{-1}(k\gamma c/u_*)^{\frac{1}{2}},$$

where c is a typical phase speed of the waves. Assuming plausible values for ϵ and c/u_*, it is shown in § 7 that T_D is of the order of minutes.

Details of the numerical procedure and computed features of the associated Langmuir convection cells will be described in another paper (Leibovich & Radhakrishnan 1977). The calculations for the horizontally averaged mean wind drift are presented here, and they show that, after a short time (about 10 units), the mean drift at the surface approaches an asymptotic value and the subsurface behaviour approaches a simple invariant pattern. A 'viscous sublayer' develops very near the surface. Below this a clearly defined logarithmic region occurs. Below the logarithmic region is a 'wake' region of nearly constant mean velocity, and a diffusion kind of cut-off exists at greater depths which brings the current to rest. As time progresses, this pattern remains essentially fixed, the only apparent changes being a progressive advance of the diffusion front and 'wake' region. The continually increasing momentum imparted by the wind goes into a steadily deepening current below the near surface equilibrium layer. This should be contrasted with the solution of the associated Rayleigh problem, in which the required momentum increase is partly accomplished by continually increasing both surface and subsurface speeds (in proportion to $t^{\frac{1}{2}}$).

The correspondance between the features predicted by the theory and phenomena actually observed in the field is remarkable. That such features also are seen in turbulent wall layers may be coincidental. Convective cells are well known to be possible, presumably owing to wave growth in unstable boundary layers (cf. Benney & Lin (1960) for the classical treatment of that problem), and should distort the flow in the way described in the present problem. Whether a similar sequence of events describes the streaks in a turbulent boundary layer is not known. The present problem is very much easier to analyse, yet it does contain the vortex stretching effects that presumably must be present in order for the streaky pattern found in the turbulent boundary layer to be produced.

2. Equations governing the time evolution

We consider an unlimited ocean of infinite depth which is at rest for times $T < 0$. At time $T = 0$, a uniform wind stress is applied at the surface, the mean position of which is described by the plane $z = 0$. The x axis is taken to be in the direction of the applied stress, the z axis is directed vertically upwards and the y axis is chosen to complete a right-handed co-ordinate system.

The wind stress will begin to generate both water waves and a water current and, of the two effects, the disturbance due to the water waves is dominant. The vorticity in the water current interacts only weakly with the water-wave motion, which may therefore be taken to be irrotational with a velocity potential ϕ.

The wind stress applied at the surface can be thought of as divided into two parts (cf. Stewart 1967). One portion may be assigned to wave drag, which leads to wave growth; the rest may be thought of as driving the wind-driven current (which is taken here to exclude the Lagrangian wave, or Stokes, drift). A precise and unambiguous division of the momentum transfer from wind to water is not simple and may be impossible in principle, but we nevertheless adopt the concept as a starting point.

Although we are interested in the response of initially quiescent water to the sudden application of a constant wind stress, we shall not consider the period of wave growth. Instead, we assume that surface gravity waves instantaneously form when the wind stress is applied, and that these waves have properties (directional energy spectrum) which do not change in time. The surface wave field will be assumed to be given, and is therefore an input to the problem.

The wind stress directly associated with current formation is therefore the only stress contribution considered, and so further reference to 'wind stress' should be understood to refer only to this portion of the applied stress. We characterize the wind stress τ_w by a water friction velocity u_*, so

$$\tau_w = \begin{cases} \rho u_*^2, & T \geqslant 0, \\ 0, & T < 0, \end{cases}$$

where ρ is the water density and T is time.

A key step in the analysis is the assumption that various components of the motion are associated with widely disparate time scales. In particular, it is assumed that, if $2\pi\sigma^{-1}$ is a typical period for surface waves, and T_c is a slow time scale required to set up the wind drift current (to be determined from the formulation), and T_t is a time scale for fluctuations small in scale compared with the wavelength of surface waves, then

$$T_t \ll 2\pi\sigma^{-1} \ll T_c.$$

The prescribed surface wave field is assumed to have a characteristic wavenumber κ ($= g^{-1}\sigma^2$ for deep water, where g is the acceleration due to gravity), and all lengths in the problem will be measured in units of κ^{-1}. The phase speed of the 'typical wave' is σ/κ. If ϵ is defined as κ times the amplitude of this wave, making ϵ a measure of wave slope, then $\epsilon\sigma\kappa^{-1}$ is representative of the water particle speed in the characteristic wave. This particular speed is taken as the unit of velocity. If time is referred to σ^{-1}, the assumptions of the previous paragraph may be

restated by asserting that the velocity vector may be represented in the multiple-time-scale form

$$\mathbf{q} = \epsilon\sigma\kappa^{-1}[\mathbf{u}_w(\mathbf{x},\tau) + \delta\mathbf{v}(\mathbf{x},\tau_s,\tau,\tau_f)], \tag{1}$$

where

$$\mathbf{u}_w(\mathbf{x},\tau) = \nabla\phi(\mathbf{x},\tau) \tag{2}$$

is the irrotational flow corresponding to the input wave field,

$$\tau_s = \epsilon_c\tau, \quad \tau_f = \epsilon_t^{-1}\tau$$

are slow and fast times defined by the small parameters

$$\epsilon_c = \sigma^{-1}T_c^{-1}, \quad \epsilon_t = \sigma T_t.$$

In (2), ∇ is the gradient with respect to the dimensionless space co-ordinates $\mathbf{x}$. The parameters ϵ, proportional to wave slope, and δ are both assumed to be small. Thus the motions set up by surface waves are assumed to dominate. The motion represented by the dimensionless velocity vector $\mathbf{v}$ includes everything else, including currents, the fluctuating interaction between currents and surface waves, and high-frequency turbulence.

Time averages are introduced, one for the 'fast' time τ_f and one for the intermediate time τ characteristic of wave fluctuations. These are defined by

$$\bar{f}(\mathbf{x},\tau_s,\tau) = \lim_{\lambda\to\infty}\frac{1}{2\lambda}\int_{-\lambda}^{\lambda} f(\mathbf{x},\tau_s,\tau,\tau_f)\,d\tau_f$$

and

$$\langle g(\mathbf{x},\tau_s)\rangle = \lim_{\lambda\to\infty}\frac{1}{2\lambda}\int_{-\lambda}^{\lambda} g(\mathbf{x},\tau_s,\tau)\,d\tau.$$

This defines the separation of $\mathbf{q}$ into means and fluctuations over the various time scales, i.e.

$$\mathbf{v} = \bar{\mathbf{v}} + \mathbf{v}'' = \langle\bar{\mathbf{v}}(\mathbf{x},\tau_s)\rangle + \mathbf{v}'(\mathbf{x},\tau_s,\tau) + \mathbf{v}''(\mathbf{x},\tau_s,\tau,\tau_f),$$

and it is assumed that $\langle\mathbf{u}_w\rangle = 0$.

The dimensionless vorticity $\boldsymbol{\omega}$ is defined by

$$\delta\epsilon\sigma\boldsymbol{\omega} = \operatorname{curl}\mathbf{q} = \epsilon\sigma\nabla\times\{\mathbf{u}_w + \delta\mathbf{v}\}$$

or

$$\boldsymbol{\omega} = \nabla\times\mathbf{v}.$$

Accounting for the multiple time scales, one obtains the vorticity equation as

$$\epsilon_c\boldsymbol{\omega}_{\tau_s} + \boldsymbol{\omega}_\tau + \epsilon_t^{-1}\boldsymbol{\omega}_{\tau_f} = \epsilon\nabla\times[(\mathbf{u}_w + \delta\mathbf{v})\times\boldsymbol{\omega}] + (\kappa^2\nu/\sigma)\nabla^2\boldsymbol{\omega}.$$

Applying the τ_f average defined earlier to this equation produces the result

$$\epsilon_c\bar{\boldsymbol{\omega}}_{\tau_s} + \boldsymbol{\omega}_\tau = \epsilon\nabla\times\{(\mathbf{u}_w\times\bar{\boldsymbol{\omega}}) + \delta(\mathbf{v}\times\bar{\boldsymbol{\omega}})\} + \epsilon\delta\nabla\times\overline{(\mathbf{v}''\times\boldsymbol{\omega}'')} + (\kappa^2\nu/\sigma)\nabla^2\bar{\boldsymbol{\omega}}.$$

The correlation of the small-scale high-frequency motion given by $\epsilon\delta\nabla\times\overline{(\mathbf{v}''\times\boldsymbol{\omega}'')}$ is the curl of the force transmitted by Reynolds stresses due to the small scales. We represent the effect of this term through a constant eddy viscosity ν_e by making the assumption that

$$\epsilon\delta\nabla\times\overline{(\mathbf{v}''\times\boldsymbol{\omega}'')} = (\kappa^2\nu_e/\sigma)\nabla^2\bar{\boldsymbol{\omega}}.$$

It is convenient to introduce the turbulent wave Reynolds number

$$R_w = \sigma/\kappa^2\nu_T,$$

where $\nu_T = \nu_e + \nu$. In cases of practical interest, it is expected that $\nu_T \approx \nu_e$. Our (quasi-laminar) vorticity equation is now

$$\epsilon_c \bar{\boldsymbol{\omega}}_{\tau_s} + \bar{\boldsymbol{\omega}}_\tau = \epsilon\nabla \times (\mathbf{u}_w \times \bar{\boldsymbol{\omega}}) + \epsilon\delta(\bar{\mathbf{v}} \times \bar{\boldsymbol{\omega}}) + R_w^{-1}\nabla^2\bar{\boldsymbol{\omega}}.$$

We assume that ϵ_c and R_w^{-1} are $o(\epsilon)$ as $\epsilon \to 0$†, and therefore write

$$\bar{\boldsymbol{\omega}} = \boldsymbol{\omega}_0 + \epsilon\boldsymbol{\omega}_1 + \text{higher-order terms},$$

$$\bar{\mathbf{v}} = \mathbf{v}_0 + \epsilon\mathbf{v}_1 + \text{higher-order terms}.$$

To lowest order the vorticity equation shows that $\boldsymbol{\omega}_0$ is independent of τ, or

$$\boldsymbol{\omega}_0 = \boldsymbol{\omega}_0(\mathbf{x}, \tau_s),$$

and the next order shows that

$$\boldsymbol{\omega}_1 = \nabla \times \left[\int^\tau \mathbf{u}_w d\tau \times \boldsymbol{\omega}_0\right].$$

Evidently $$\langle\bar{\boldsymbol{\omega}}\rangle = \boldsymbol{\omega}_0 + o(\epsilon)$$

and $$\bar{\boldsymbol{\omega}}' = \epsilon\boldsymbol{\omega}_1 + o(\epsilon).$$

Applying the τ-average to the vorticity equation gives the slow-time evolution equation

$$\epsilon_c\boldsymbol{\omega}_{\tau_s} = \epsilon^2\nabla \times \langle\mathbf{u}_w \times \boldsymbol{\omega}_1\rangle + \epsilon\delta\nabla \times (\mathbf{v}_0 \times \boldsymbol{\omega}_0) + R_w^{-1}\nabla^2\boldsymbol{\omega}_0 + O(\epsilon^3, \epsilon^2\delta, \epsilon R_w^{-1}). \tag{3}$$

Craik & Leibovich (1976) show that for any $\mathbf{u}_w$ that satisfies the assumptions already stated

$$\nabla \times \langle\mathbf{u}_w \times \boldsymbol{\omega}_1\rangle = \boldsymbol{\omega}_0 . \nabla\mathbf{v}_s - \mathbf{v}_s . \nabla\boldsymbol{\omega}_0,$$

where

$$\mathbf{v}_s \equiv \left\langle \left(\int^t \mathbf{u}_w d\tau\right) . \nabla\mathbf{u}_w \right\rangle. \tag{4}$$

This expression may be identified (cf. Phillips 1966) as the Stokes wave drift, as found by Longuet-Higgins (1953). Although the wave drift is a Lagrangian concept, it arises here in a purely Eulerian framework. We shall nevertheless refer to $\mathbf{v}_s$ as the wave drift.

We shall now assume that ϵ_c, ϵ^2, $\epsilon\delta$, and R_w^{-1} are of comparable magnitude, and that the error term indicated in (3) is negligible when compared with them, so that it may be omitted. Without loss of generality, we shall set

$$\epsilon_c = \epsilon\delta,$$

which is equivalent to identifying the slow time scale with the convective time scale corresponding to current motions in the plane perpendicular to the wind.

† A self-consistent and rational development is sought. The assumptions made at this point link the small parameters in one particular way and are appropriate under a set of physical conditions. Other developments appropriate to other physical circumstances may also be possible.

Incorporating (4) and the remarks above into (3) and then dividing by ϵ_c gives the equation for $\boldsymbol{\omega}_0$ as

$$\partial\boldsymbol{\omega}_0/\partial\tau_s + \mathbf{v}_0 . \nabla\boldsymbol{\omega}_0 - \boldsymbol{\omega}_0 . \nabla\mathbf{v}_0 = (\epsilon_c R_w)^{-1}\nabla^2\boldsymbol{\omega}_0 + (\epsilon/\delta)(\boldsymbol{\omega}_0 . \nabla\mathbf{v}_s - \mathbf{v}_s . \nabla\boldsymbol{\omega}_0). \tag{5}$$

It is assumed that the wave field leads to a wave drift that is unidirectional and oriented in the direction of the applied wind stress (x). Since $\nabla . \mathbf{v}_s = 0$, we have

$$\mathbf{v}_s = (u_s(y, z), 0, 0).$$

Furthermore, the symmetry of the problem requires $\mathbf{v}_0$ to be independent of x. Let the $\mathbf{v}_0$ and $\boldsymbol{\omega}_0$ components be designated by

$$\mathbf{v}_0 = (u, v, w), \quad \boldsymbol{\omega}_0 = (\xi, \eta, \zeta).$$

As a consequence of the x independence,

$$\boldsymbol{\omega}_0 . \nabla u \equiv 0$$

and

$$\eta = \partial u/\partial z, \quad \zeta = -\partial u/\partial y.$$

The x component of the vorticity equation is therefore

$$\frac{\partial\xi}{\partial\tau_s} + v\xi_y + w\xi_z = (\epsilon_c R_w)^{-1}\nabla^2\xi + \frac{\epsilon}{\delta}\left(u_z\frac{\partial u_s}{\partial y} - u_y\frac{\partial u_s}{\partial z}\right). \tag{6}$$

The term involving the wave drift does not appear in the other two components of the vorticity equation. Upon noting that continuity demands

$$v_y + w_z = 0, \tag{7}$$

and that because $\boldsymbol{\omega}_0$ is solenoidal

$$\eta_y + \zeta_z = 0,$$

the y and z components of the vorticity equation may be integrated to produce the x-momentum equation

$$u_{\tau_s} + vu_y + wu_z = (\epsilon_c R_w)^{-1}\nabla^2 u. \tag{8}$$

Equation (7) may be dispensed with by introducing a stream function for the y, z plane with

$$v = \psi_z, \quad w = -\psi_y. \tag{9}$$

Then

$$\psi_{yy} + \psi_{zz} = \nabla^2\psi = -\xi \tag{10}$$

and (6), (8), (9) and (10) govern the current system, subject to the specification of u_s and boundary conditions.

Under the assumptions adopted here, Craik & Leibovich (1976) show that the boundary conditions

$$\left.\begin{aligned} \psi(y, 0, t) = \psi_{zz}(y, 0, t) = 0, \\ u \to 0, \ \psi \to 0 \quad \text{as} \quad z \to -\infty \end{aligned}\right\} \tag{11}$$

are appropriate. The surface stress boundary condition can be expressed in a form that is consistent with the employment of an eddy viscosity as follows:

$$\nu_T \epsilon\delta\sigma u_z(y, 0, t) = u_*^2,$$

or

$$u_z(y, 0, t) = u_*^2/\nu_T\sigma\epsilon\delta.$$

The applied stress is the primary driving force in the problem, and we recognize this by selecting δ so that

$$u_z(y, 0, t) = 1. \tag{12}$$

Thus

$$\delta = u_*^2/\nu_T \sigma\epsilon. \tag{13}$$

This identification of δ determines the current speed scale in terms of parameters that are assumed to be given. The time scale for current formation is also determined by the choice of δ, since on using (13) we have

$$\epsilon_c = \epsilon\delta = u_*^2/\nu_T \sigma. \tag{14}$$

The problem has now been reduced to solving the governing equations (6), (8), (9) and (10) subject to the boundary conditions (11) and (12). The differential equations depend upon the two parameters

$$\epsilon_c R_w = \frac{u_*^2}{\nu_T \sigma} \frac{\sigma}{\kappa^2 \nu_T} \quad \text{and} \quad \frac{\epsilon}{\delta} = \frac{\epsilon^2 \sigma \nu_T}{u_*^2}.$$

The number of independent parameters can be reduced to one by redefining ξ and τ_s as

$$\xi = (\epsilon/\delta)^{\frac{1}{2}}\, \Omega, \quad \tau_s = (\delta/\epsilon)^{\frac{1}{2}} t, \tag{15a, b}$$

and, since the velocity components and stream function in the cross-plane are determined by ξ, we redefine them in the same way:

$$(v, w, \psi) = (\epsilon/\delta)^{\frac{1}{2}} (V, W, \Psi). \tag{15c}$$

Since ϵ and δ are assumed to be of comparable order, this rescaling does not change the asymptotic characteristics of the problem. With the transformations (15) introduced, the governing equations are modified as follows:

$$u_t + V u_y + W u_z = La \nabla^2 u, \tag{16a}$$

$$\Omega_t + V \Omega_y + W \Omega_z = La \nabla^2 \Omega + u_z u_{sy} - u_y u_{sz}, \tag{16b}$$

$$\nabla^2 \Psi = -\Omega, \tag{16c}$$

$$V = \Psi_z, \quad W = -\Psi_y, \tag{16d}$$

$$La = (\delta/\epsilon)^{\frac{1}{2}} (\epsilon_c R_w)^{-1} = (u_*/\epsilon)\, (\sigma \nu_T)^{-\frac{1}{2}} \kappa^2 \nu_T^2 / u_*^2, \tag{16e}$$

with boundary conditions

$$(u, V, W) \to 0 \quad \text{as} \quad z \to -\infty, \tag{17a}$$

$$\Psi(y, 0, t) = \Psi_{zz}(y, 0, t) = \Omega(y, 0, t) = 0, \tag{17b}$$

$$u_z(y, 0, t) = 1, \tag{17c}$$

and the initial conditions $u(y, z, 0) = \Psi(y, z, 0) = 0$. The one parameter remaining explicitly, La, is defined in (16*e*).

Retracing the sequences of scaling transformations used to arrive at (14)–(16), we note that the velocity vector $\mathbf{U}_c$ of the current is given in terms of u, V, W, by

$$\mathbf{U}_c = \epsilon\sigma\kappa^{-1}\delta\mathbf{v} = (u_*^2/\nu_T \kappa)\, (u, 0, 0) + (\epsilon u_*/\nu_T \kappa)\, (\sigma \nu_T)^{\frac{1}{2}} (0, V, W), \tag{18}$$

the unit of time in (15), in dimensional terms, is the convective time (based on velocities in the y, z plane)

$$\epsilon_c^{-1}\beta^{-\frac{1}{2}}\sigma^{-1} = \sigma^{-1}(\nu_T\sigma)^{\frac{1}{2}}/\epsilon u_*, \tag{19a}$$

and the unit of length is κ^{-1}.

The dimensionless problem for u, V, W thus has been reduced to one depending on the parameter La and whatever parameters might appear in the 'wave drift' speed u_s. In the simplest case, the one to be considered in this paper, u_s will be seen to depend only on an angle describing the orientation of two wavenumber vectors of the surface waves. All other information governing the problem resides in La, which might appropriately be called the 'Langmuir number' in view of the history of the problem. The Langmuir number is related to wave properties, stress, etc., as follows:

$$La = (\nu_T\kappa^2/u_*)\,(\sigma\nu_T)^{\frac{1}{2}}/\epsilon\sigma. \tag{19b}$$

Noting that the convective velocity scale is $(\sigma\nu_T)^{\frac{1}{2}}\epsilon u_*/\nu_T\kappa$, we see that the Langmuir number has the usual interpretation of an inverse Reynolds number as a ratio of 'viscous' force to inertial forces, or

$$(\rho\nu_T\kappa^2 \times \text{velocity})/(\rho\kappa(\sigma\nu_T)^{\frac{1}{2}}\,(\epsilon u_*/\nu_T\kappa) \times \text{velocity}).$$

Another interpretation of La is as the ratio of the rate of diffusion of vorticity to the rate of production of streamwise vorticity by vortex stretching accomplished solely by the wave drift. Since the dimensional wave drift is of order $\epsilon^2\sigma/\kappa$, the rate of production of streamwise vorticity is

$$\frac{u_*^2}{\nu_T\kappa} \times \kappa \times \frac{\epsilon^2\sigma}{\kappa}$$

while the rate of diffusion of streamwise vorticity is

$$\nu_T \frac{\epsilon u_*}{\nu_T\kappa}\,(\sigma\nu_T)^{\frac{1}{2}} \times \kappa^2$$

and the ratio of the latter to the former is La. By comparing the two interpretations it is seen that the convective velocity scale has been chosen so as to balance inertial effects against vortex stretching.

3. Forcing by monochromatic waves

In order to complete the statement of the mathematical problem, boundary conditions on two boundaries y = constant are required. The irrotational wave field is assumed to be given, and the wave drift $u_s(y, z)$ is therefore determined. If u_s is periodic in y, it is natural to impose the condition that the flow be periodic in y with the same period as u_s. The y boundary conditions are prescribed by the periodicity condition, and the setting of the problem posed by (15) and (16) is therefore completed.

The superposition of two monochromatic wave trains is perhaps the simplest wave drift that is periodic in y. If the wave trains each have the same amplitude a, frequency σ and wavenumber κ, and propagate at equal and opposite angles θ to

the wind direction, then the combined wave field has the (dimensional) velocity potential

$$(2a\sigma/\kappa)\, e^{\kappa z} \cos(\kappa y \sin\theta) \cos(\kappa x \cos\theta - \sigma t).$$

The (again dimensional) wave drift corresponding to this velocity potential is

$$2\sigma a^2 \kappa \cos\theta\, e^{2\kappa z}[1 + \cos^2\theta \cos(2\kappa y \sin\theta)]. \tag{20a}$$

We take the dimensionless wave-slope parameter ϵ to be $\epsilon = a\kappa$. For a monochromatic wave of amplitude a, the wave slope is ϵ/π. Note that the observed wave amplitudes will be twice a, so that the wave slopes that occur with the postulated wave system will be $(2\epsilon/\pi)\cos\theta$.

Since u_s is periodic with period $\pi/(\kappa \sin\theta)$, we require the motion to be periodic in y with the same period. If $y = 0$ corresponds to a cell boundary, then the motion is symmetric in u and antisymmetric in Ψ about $y = 0$ and $y = \pi/(2\kappa \sin\theta)$. Consequently we may confine attention to the single cell $0 \leqslant y \leqslant \pi/(2\kappa \sin\theta)$. If we take $L = \pi/(2\sin\theta)$, then, in dimensionless variables, a single cell is located in $0 \leqslant y \leqslant L$, and the dimensionless conditions that must be imposed on the lateral cell boundaries to supplement (16) are

$$\Psi(0,z,t) = \Psi(L,z,t) = \Omega(0,z,t) = \Omega(L,z,t) = \frac{\partial u}{\partial y}(0,z,t) = \frac{\partial u}{\partial y}(L,z,t) = 0.$$

The dimensionless form of the wave drift (20a) is

$$u_s = 2\cos\theta\, e^{2z}[1 + \cos^2\theta \cos(2y \sin\theta)]. \tag{20b}$$

The remainder of the paper is devoted to motions produced by the action of wave drift currents of the form (20).

4. The horizontally averaged drift current

A solution $\mathbf{U}_c$ for the Langmuir current system (see (18)) will be a periodic function of y. After $\mathbf{U}_c$ has been obtained, its average over one period in y can be computed to yield the horizontally averaged drift current (one y period is $2L$ and comprises two counter-rotating cells defined in the last section). By the symmetry of the problem, the only non-zero component of this average is in the wind direction, and is given by

$$\overline{U}_c \equiv \frac{1}{2L}\int_0^{2L} \left(\frac{u_*^2}{\nu_T \kappa}\right) u(y,z,t)\, dy \equiv \frac{u_*^2}{\nu_T \kappa}\, \overline{u}(z,t). \tag{21a}$$

The mean velocity component $\overline{u}(z,t)$ satisfies the equation

$$\partial \overline{u}/\partial t = La\, \partial^2 \overline{u}/\partial z^2 - (\overline{Wu})_z, \tag{21b}$$

where

$$-\overline{Wu} = -\frac{1}{2L}\int_0^{2L} W(y,z,t)\, u(y,z,t)\, dy \tag{21c}$$

is the Reynolds stress due to the y fluctuations. The mean velocity $\overline{u}$ is dealt with here in two ways. First, the complete set of equations for the wind drift currents and Langmuir circulations is solved numerically, and the resulting u component

is averaged over a cell; the Reynolds stress is found at the same time, for reference purposes. Second, an approximate solution is found for $(La\,t)^{\frac{1}{2}}$ small; a Reynolds stress $-\overline{Wu}$ is calculated and substituted into (21), which is then solved for $\bar{u}$.

Motion for small time

The initial condition is a state of rest, and the motion for small time is therefore described by the linearized version of (16). An approximate solution valid for small time is sought that can describe the first effects of convection on the horizontally averaged current.

An artificial small parameter $\hat{\epsilon}$ and a new time τ are introduced to order the perturbation through the relation

$$t = \hat{\epsilon}(La)^{-1}\tau. \tag{22}$$

The initial disturbances are transmitted by diffusion, and the leading approximation to $u(y, z, t)$ is determined by a Rayleigh problem with unit applied stress. As a result, the vertical co-ordinate should be scaled by $\hat{\epsilon}$ as well, so we introduce the vertical co-ordinate Z by

$$z = \hat{\epsilon}^{\frac{1}{2}}Z,$$

and let $$\tilde{\eta} = z/2(La\,t)^{\frac{1}{2}} = Z/2(\tau)^{\frac{1}{2}}.$$

The boundary condition

$$[\partial u/\partial z]_{z=0} = 1 = \hat{\epsilon}^{-\frac{1}{2}}[\partial u/\partial Z]_{z=0}$$

shows that u is $O(\hat{\epsilon}^{\frac{1}{2}})$ for small $\hat{\epsilon}$; the vorticity equation shows that Ω is $O(\hat{\epsilon})$ for small $\hat{\epsilon}$, and it follows that Ψ is $O(\hat{\epsilon}^2)$. Therefore we set

$$u = \hat{\epsilon}^{\frac{1}{2}}u_0(y, Z, \tau) + \Delta_1(\hat{\epsilon})\,u_1(y, Z, \tau) + \Delta_2(\hat{\epsilon})\,u_2(y, Z, \tau) + \ldots,$$

$$\Omega = \hat{\epsilon}\Omega_0(y, Z, \tau) + g_1(\hat{\epsilon})\,\Omega_1(y, Z, \tau) + \ldots,$$

$$\Psi = \hat{\epsilon}^2\Psi_0(y, Z, \tau) + \hat{\epsilon}g_1(\hat{\epsilon})\,\Psi_1(y, Z, \tau) + \ldots.$$

When these expansions are substituted into (16), the equation for u_0 is

$$\partial u_0/\partial\tau - \partial^2 u_0/\partial Z^2 = 0,$$

with boundary conditions

$$\frac{\partial u_0}{\partial Z}(y, 0, \tau) = 1 \quad \text{and} \quad u_0 \to 0 \quad \text{as} \quad Z \to \infty,$$

and the initial condition

$$u_0(y, Z, 0) = 0.$$

This is a Rayleigh problem, and it has the solution

$$u_0 = 2(\tau)^{\frac{1}{2}}f_0(\tilde{\eta}), \tag{23}$$

where $$f_0(\tilde{\eta}) = \pi^{-\frac{1}{2}}\exp(-\tilde{\eta}^2) + \tilde{\eta}\,\mathrm{erfc}(-\tilde{\eta}). \tag{24}$$

We note that the equation satisfied by f_0 is

$$f_0'' + 2\tilde{\eta}f_0' - 2f_0 = 0, \tag{25}$$

and the boundary conditions are

$$f_0'(0) = 1, \quad f_0(-\infty) = 0.$$

Primes denote derivatives with respect to $\tilde{\eta}$.

The equation satisfied by Ω_0 is

$$\frac{\partial \Omega_0}{\partial \tau} - \frac{\partial^2 \Omega_0}{\partial Z^2} = -\frac{4r^3 s}{La} \sin(2sy) f_0', \tag{26}$$

where we have set

$$r \equiv \cos\theta, \quad s \equiv \sin\theta.$$

In deriving (26), we have expanded the factor $\exp(2z) = \exp(2\hat{\epsilon}^{\frac{1}{2}}Z)$, which occurs in the Stokes drift u_s, in powers of $\hat{\epsilon}^{\frac{1}{2}}$, and only the lowest-order term appears in (26). Set

$$\Omega_0 = (4r^3 s/La)(\sin 2sy)\, G_0(Z, \tau), \tag{27}$$

then G_0 satisfies homogeneous boundary conditions at $Z = 0$ and $Z = -\infty$, and vanishes at $t = 0$ for all Z. The solution is readily found to be

$$G_0 = \tfrac{1}{2} Z u_0(Z, \tau) = 2\tau\tilde{\eta} f_0(\tilde{\eta}). \tag{28}$$

The equation for Ψ_0' is

$$\partial^2 \Psi_0'/\partial Z^2 = -\Omega_0 = -(8r^3 s/La)(\sin 2sy)\, \tau\tilde{\eta} f_0(\tilde{\eta}). \tag{29}$$

Ψ_0' can be set equal to

$$\Psi_0' = -(32r^3 s/La)(\sin 2sy)\, \tau^2 h_0(\tilde{\eta}), \tag{30}$$

and (29) will be satisfied provided

$$h_0'' = \tilde{\eta} f_0(\tilde{\eta}),$$

or

$$h_0(\tilde{\eta}) = C_1 + C_2\tilde{\eta} + \int_{-\infty}^{\tilde{\eta}} d\mu \int_{-\infty}^{\mu} \nu f_0(\nu)\, d\nu. \tag{31}$$

The boundary conditions require $h_0(0) = h_0(-\infty) = 0$, but it is not possible to satisfy both conditions, and the boundary condition at infinity must be corrected by the construction of an outer solution. We take $C_2 = 0$ to prevent an unmatchable limit, and choose C_1 to satisfy the surface boundary condition. The integrals in (31) may be shown to yield

$$h_0 = C_1 + \tfrac{1}{16}\{(-1 + \tfrac{2}{3}\tilde{\eta}^2)\, df_0/d\tilde{\eta} + \tfrac{2}{3}\tilde{\eta}(-1 + 2\tilde{\eta}^2) f_0\}. \tag{32}$$

Recalling that $df_0/d\tilde{\eta} = 1$ at $\tilde{\eta} = 0$, the constant C_1 must be chosen to be

$$C_1 = \tfrac{1}{16}. \tag{33}$$

To satisfy the boundary condition at infinity, we must correct the solution above in the sense of matched asymptotic expansions. The inner solution that we have constructed has the limit

$$\Psi' \to -\hat{\epsilon}^2 (2r^3 s/La)(\sin 2sy)\, \tau^2$$

as $\hat{\epsilon}_2^{\frac{1}{2}} \to 0$, z fixed. Since the vorticity $\Omega \to 0$ exponentially for fixed z as $\hat{\epsilon} \to 0$, the outer solution Ψ' satisfies Laplace's equation

$$\Psi'_{zz} + \Psi'_{yy} = 0.$$

The boundary condition on $\Psi(y,z,t)$ required to match the inner solution is

$$\Psi(y,0,\tau) = -2\hat{\epsilon}^2\tau^2(r^3s/La)\sin 2sy.$$

The required outer solution is then

$$\Psi(y,z,\tau) = -2\hat{\epsilon}^2\tau^2(r^3s/La)\,e^{2sz}\sin 2sy. \tag{34}$$

Consideration of the equation for u_1 shows that $\Delta_1(\hat{\epsilon}) = \hat{\epsilon}^3$, and that

$$\frac{\partial u_1}{\partial\tau} - \frac{\partial^2 u_1}{\partial Z^2} = \frac{1}{La}\frac{\partial\Psi_0}{\partial y}\frac{\partial u_0}{\partial Z}. \tag{35}$$

By reference to (23) and (30), it is seen that if we take u_1 to be

$$u_1 = (64r^3s^2/La^2)(\cos 2sy)\,\tau^3 f_1(\tilde{\eta}), \tag{36}$$

then f_1 satisfies the equation

$$f_1'' + 2\tilde{\eta}f_1' - 12f_1 = 4h_0f_0' \tag{37a}$$

and the boundary conditions

$$f_1'(0) = 0 = f_1(-\infty). \tag{37b}$$

The approximation already found for Ψ, together with the solution (36) for u_1, is sufficient to evaluate the lowest-order non-zero contribution to the Reynolds stress $-\overline{Wu}$ in (21),

$$-\overline{Wu} = \overline{u_1(\partial\Psi_0/\partial y)} = -\tfrac{1}{2}(4r)^6 s^4 La^{-3}(\hat{\epsilon}\tau)^5 f_1(\tilde{\eta})\,h_0(\tilde{\eta}). \tag{38}$$

If (38) is substituted into (21), the resulting equation in τ, Z co-ordinates is

$$\frac{\partial\bar{u}}{\partial\tau} - \frac{\partial^2\bar{u}}{\partial Z^2} = -\frac{(4r)^6 s^4}{2La^4}\hat{\epsilon}^{\frac{11}{2}}\tau^5\frac{\partial f_1 h_0}{\partial Z} = -\frac{(4r)^6 s^4}{4La^4}\hat{\epsilon}^{\frac{11}{2}}\tau^{\frac{9}{2}}\frac{df_1h_0}{d\tilde{\eta}}. \tag{39}$$

The horizontally averaged current $\bar{u}$ to order $\hat{\epsilon}^{\frac{11}{2}}$ satisfies (39), which may be solved by setting

$$\bar{u} = (\hat{\epsilon}\tau)^{\frac{1}{2}}[2f_0(\tilde{\eta}) + (\hat{\epsilon}\tau)^5(4r)^6 s^4 La^{-4}f_2(\tilde{\eta})]. \tag{40}$$

The function f_2 is the solution to the problem

$$f_2'' + 2\tilde{\eta}f_2' - 22f_2 = (f_1h_0)', \tag{41a}$$

$$f_2'(0) = f_2(-\infty) = 0. \tag{41b}$$

The functions f_1 and f_2 may readily be found by the method of variation of parameters:

$$f_1(\tilde{\eta}) = -(\phi_6(0)\,\theta_5(0))^{-1}\Big\{\phi_6(\tilde{\eta})\int_{-\infty}^{\tilde{\eta}}\theta_6(\nu)\,R_1(\nu)\exp(\nu^2)\,d\nu + \theta_6(\tilde{\eta})\int_{\tilde{\eta}}^{0}\phi_6(\nu)\,R_1(\nu)\exp(\nu^2)\,d\nu\Big\}, \tag{42a}$$

$$R_1(\tilde{\eta}) = 4h_0f_0', \tag{42b}$$

$$f_2(\tilde{\eta}) = (\phi_{10}(0)\,\theta_{11}(0))^{-1}\Big\{\phi_{11}(\tilde{\eta})\int_{-\infty}^{\tilde{\eta}}\theta_{11}(\nu)\,R_2(\nu)\exp(\nu^2)\,d\nu + \theta_{11}(\tilde{\eta})\Big[\int_{\tilde{\eta}}^{0}\phi_{11}(\nu)\,R_2(\nu)\exp(\nu^2)\,d\nu - \int_{-\infty}^{0}\theta_{11}(\nu)\,R_2(\nu)\exp(\nu^2)\,d\nu\Big]\Big\}, \tag{43a}$$

$$R_2(\tilde{\eta}) = (f_1(\tilde{\eta})\,h_0(\tilde{\eta}))'. \tag{43b}$$

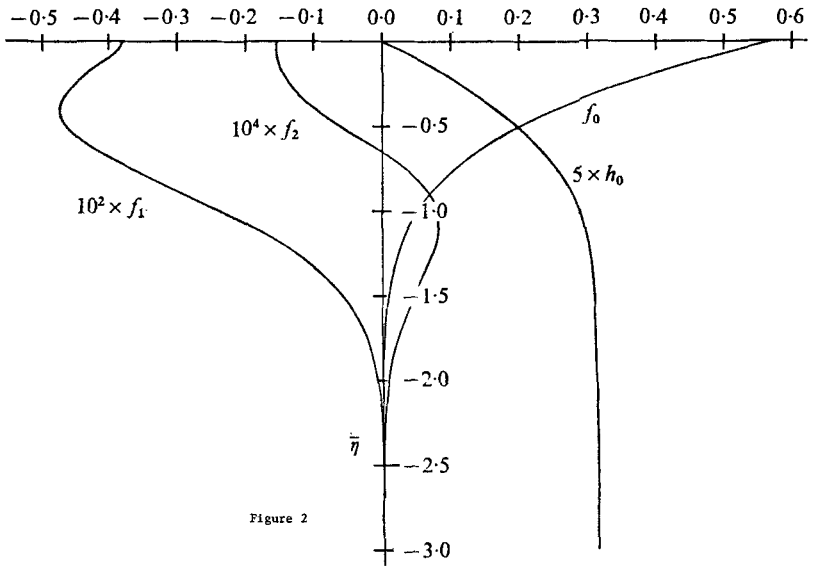

FIGURE 2. Functions arising in the small time solution.

The functions ϕ_m and θ_m, $m = 5$, 6, 10, 11, are independent solutions of the homogeneous equation

$$g_m'' + 2\tilde{\eta} g_m' - 2m g_m = 0. \tag{44}$$

The solution for f_1 was found by numerically evaluating the formal solution (42). To avoid the need to differentiate to find $R_2(\tilde{\eta})$, (43) was integrated once by parts before f_2 was numerically evaluated. The formula used to compute f_2 was then

$$f_2 = -24[\phi_{10}(0)\,\theta_{11}(0)]^{-1}\left\{\phi_{11}(\tilde{\eta})\int_{-\infty}^{\tilde{\eta}} \theta_{12} R_3 \exp(\nu^2)\,d\nu + \theta_{11}(\tilde{\eta})\left[\int_{\tilde{\eta}}^{0} \phi_{12} R_3 \exp(\nu^2)\,d\nu - \int_{-\infty}^{0} \theta_{12} R_3 \exp(\nu^2)\,d\nu\right]\right\}, \tag{45a}$$

$$R_3(\tilde{\eta}) = h_0(\tilde{\eta}) f_1(\tilde{\eta}). \tag{45b}$$

In deriving (45), the properties of the ϕ_m and θ_m, and the fact that $h_0(0) = 0$ were used. The numerical method used to evaluate (43) and (45), together with the necessary information concerning the functions ϕ_m, θ_m, is given in the appendix.

The functions f_0, h_0, f_1, and f_2 are displayed in figure 2. The redistribution of momentum due to vertical mixing accomplished by the Langmuir cells can be inferred from the curves for f_0 and f_2. It should be remembered that u_0, represented by f_0, is the velocity profile that would obtain in the absence of vertical mixing. From the form of f_2, it is seen that the mixing lowers the surface speed and increases the speed at greater depth.

Finite-difference solutions for larger time

A series of calculations using finite-difference approximations to the full non-linear equations (16) has been carried out for $\theta = 30°$ and $\theta = 15°$ with $La = 0{\cdot}1$ and $0{\cdot}01$. The finite-difference approximations are explicit, employ second

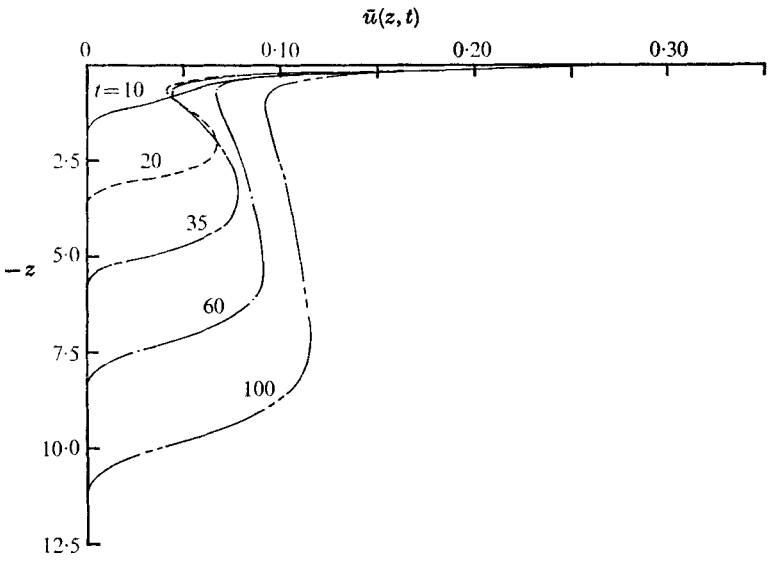

FIGURE 3. Development of the (dimensionless) mean current profiles as a function of time as obtained from the finite-difference solution for $\theta = 30°$, $La = 0{\cdot}01$.

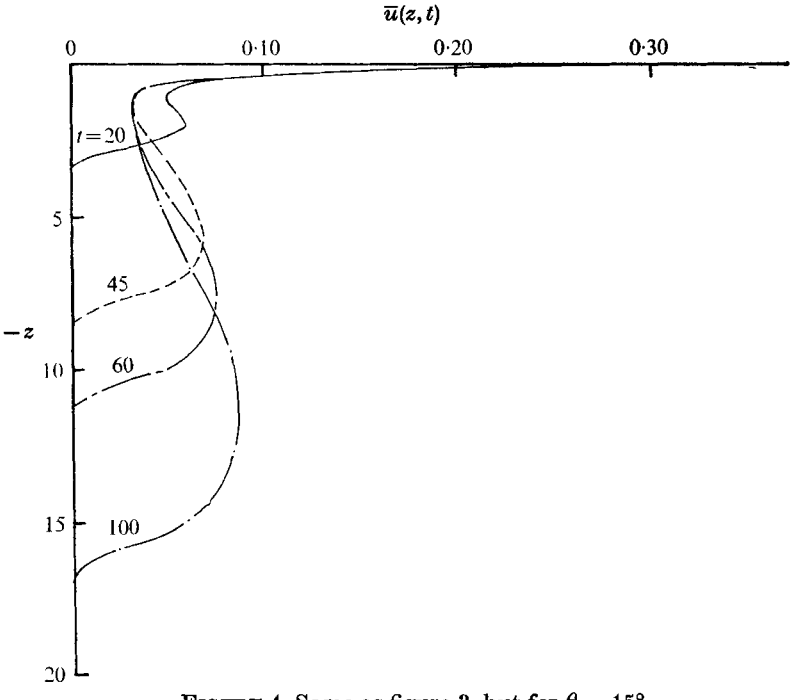

FIGURE 4. Same as figure 3, but for $\theta = 15°$.

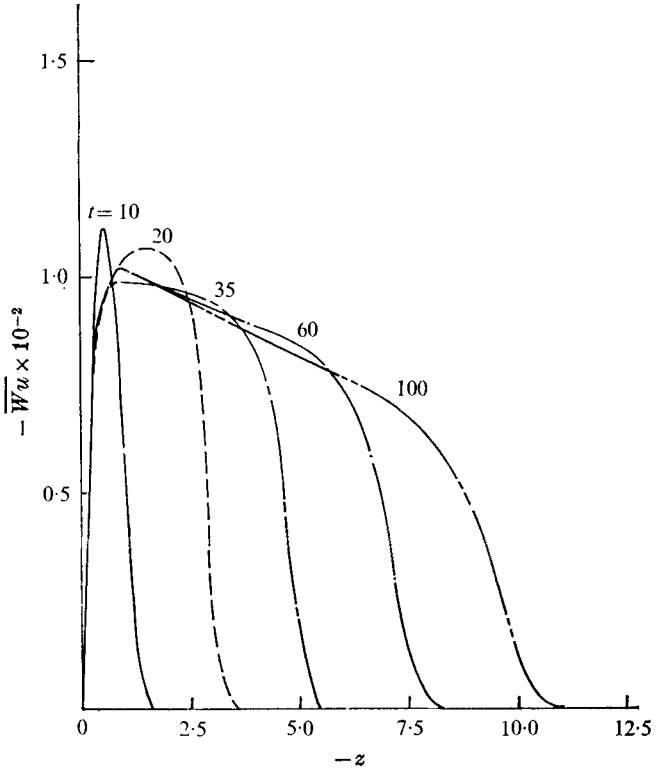

FIGURE 5. Reynolds stress for the case depicted in figure 3.

upwind differencing for the advection terms, forward time differences, and central differences for the Laplacian operator. The Poisson equation for Ψ is solved by successive over-relaxation. The algorithms are now standard and are described, for example, in the book by Roache (1972). Spatial differences required for the vortex-stretching term that acts as a forcing function for the vorticity equation employ a combination of forward and backward differences. We shall not discuss the numerical procedures here; a full account will be given in Leibovich & Radhakrishnan (1977).

The initial-value problem posed in §§ 2 and 3 with the wave drift (20) was solved, and the detailed results for the Langmuir cells will be described in Leibovich & Radhakrishnan (1977). After a solution for $u(y, z, t)$ was obtained, a numerical integration was carried out across the Langmuir cell, and the horizontally averaged wind drift $\bar{u}(z, t)$ was calculated according to (21*a*). The Reynolds stress (21*c*) was also calculated by averaging the product $-Wu$ in the same fashion. The evaluation of the wind drift current and the instantaneous Reynolds stresses that resulted from these calculations are presented here.

The wind drifts $\bar{u}(z, t)$ are plotted in figure 3 for the case $La = 0{\cdot}01$, $\theta = 30°$ and in figure 4 for $\theta = 15°$, $La = 0{\cdot}01$; the corresponding Reynolds stresses $-\overline{Wu}$, calculated from the finite-difference solutions, are presented in figures 5 and 6. Our calculations for larger values of La have not been carried out for a sufficiently

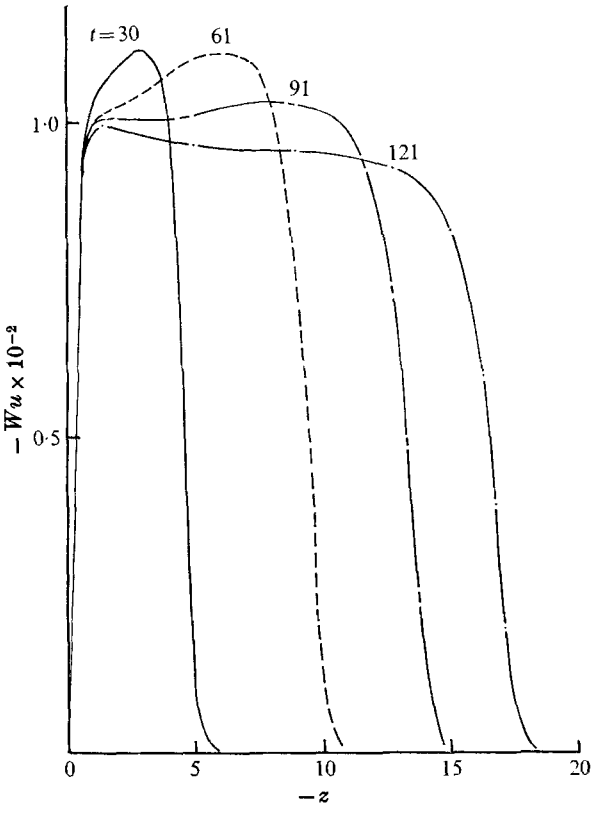

FIGURE 6. Reynolds stress for the case depicted in figure 4.

long time period to discern a clear pattern and will not be described. To facilitate the discussion, a streamline plot for $\theta = 15°$, $t = 30$ is presented in figure 7. (Additional streamline plots will be given in Leibovich & Radhakrishnan 1977.)

The effect of mixing on the profiles shown in figures 3 and 4 is pronounced. The relative minimum in $\overline{u}$ that occurs at a depth $z = z_m$ is one feature that arises from the convective action of the Langmuir cells. The solution shows that z_m is independent of time ($z_m \approx -1$) and seems to correspond to the effective extent of the x vorticity generation. This region is determined by the wavelength of the surface waves, since generation of x vorticity is accomplished by vortex-line stretching due to wave effects.

Some insight into the minimum in $\overline{u}$ may be gained by considering the averaged equation (21*b*) in conjunction with the curves of Reynolds stress given in figures 5 and 6. Near the peak in Reynolds stress, which corresponds closely to the location of the minimum of $\overline{u}$, the net force exerted by the Reynolds stress will be small. Consequently, the rate of growth of $\overline{u}$ will be determined by 'viscous' stresses, which are weak for small La. Thus the minimum of $\overline{u}$ will grow slowly. At depths greater than z_m, $-\partial(\overline{Wu})/\partial z > 0$ and $La\,\partial^2\overline{u}/\partial z^2$ is negligible: therefore (21*b*) may be approximated by

$$\partial\overline{u}/\partial t = -\partial\overline{Wu}/\partial z > 0,$$

so $\overline{u}$ grows for $z < z_m$, and the bulge in the $\overline{u}$ profile is formed.

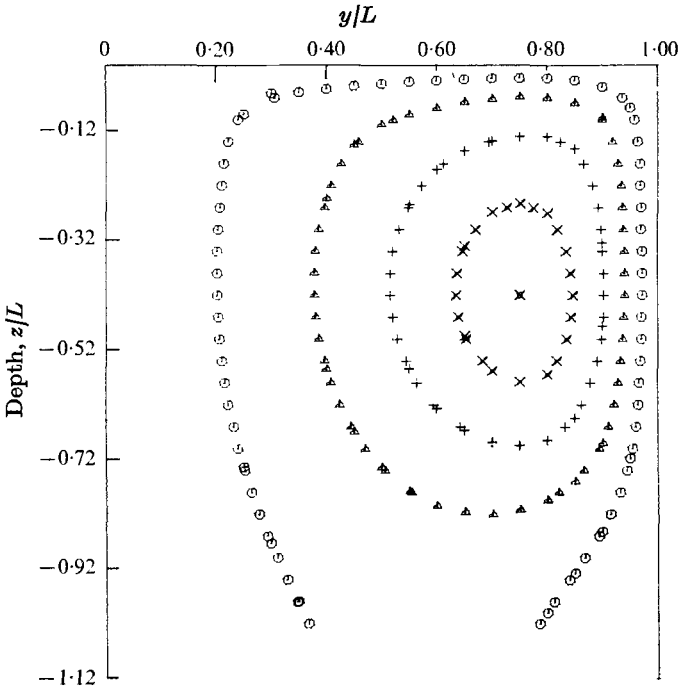

FIGURE 7. Streamline pattern for $\theta = 15°$, $t = 30$ and $La = 0{\cdot}01$. The motion is clockwise. ⊙, $\Psi = 0{\cdot}02$; △, $\Psi = 0{\cdot}04$; +, $\Psi = 0{\cdot}06$; ×, $\Psi = 0{\cdot}08$.

To explore further the origin of the minimum in $\bar{u}$, sections of the $u(y, z, t)$ profile are presented in figures 8 (*a–c*). Figure 8 (*a*) shows u at a section through the upwelling cell boundary $y = 0$, figure 8 (*b*) shows u at a section through the centre of the cell at $y = \frac{1}{2}L$, and figure 8 (*c*) shows u at the downwelling cell boundary $y = L$. The upwelling fluid transports low-momentum fluid upwards, this effect being clearly seen in figure 8 (*a*), where u is very small except in the layer of fluid near the surface, which is forced directly by the applied stress. The effect of a strong downward transport of high x-momentum fluid is clear from figure 8 (*c*). The origin of the bulges in the $\bar{u}$ profiles is revealed in figure 8 (*b*). They arise from the fact that most of the transport in the centre sections of the cell is horizontal, with relatively high x-momentum fluid originating from the downwelling jet entering the centre regions of the cell at depths below the cell centre. Close to the surface, slower moving fluid moves toward the centre from the vicinity of the upwelling cell boundary.

Presumably, if the diffusion represented by the quasi-viscous term $La\,\bar{u}_{zz}$ is allowed a sufficiently long time to act, the jet and the bulge it creates will be smoothed out, and a more conventional-looking boundary-layer profile would replace $\bar{u}$. The dimensionless diffusion time based upon cell width L is L^2/La. For $\theta = 30°$, this diffusion time is 989, while for $\theta = 15°$, the diffusion time is 3683. Therefore, in our calculations the lateral smoothing which presumably will eventually take place is not yet effective.

The motion near the surface rapidly develops a quasi-equilibrium structure

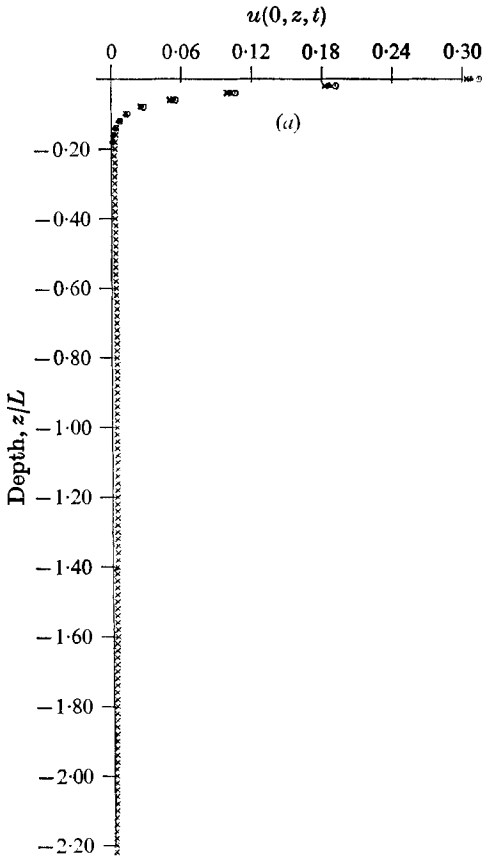

FIGURE 8(a). For legend see facing page.

that changes only slowly with time. One measure of this process is the rapid approach of $\overline{u}(0,t)$ to an asymptotic value. Figure 9 illustrates this point. For all practical purposes, $\overline{u}(0,t)$ reaches its asymptotic value within ten dimensionless time units.

Interesting features of the near-surface equilibrium structure are brought out by replotting figures 3 and 4 on semi-log paper. This has been done in figures 10 and 11, which show the velocity defects $\overline{u}(0,t)-\overline{u}(z,t)$. These figures show that a portion of the profile is linear in $\log|z|$. By analogy with the turbulent boundary layer, this might be called an inertial sublayer; it clearly arises because the Reynolds stress has much the same shape as it does in a turbulent boundary layer. A thin 'viscous sublayer' joins the surface to the inertial sublayer.

To display this feature more clearly, we have indicated the velocity defect for all computed interior z points up to its local maximum. Beyond the local maximum, a smooth curve connects the remaining computed points, which are not individually marked. Straight lines pass precisely through all points in the interval between $-z = 0{\cdot}12$ and $-z = 0{\cdot}30$ in figure 10 for each instant of time. The

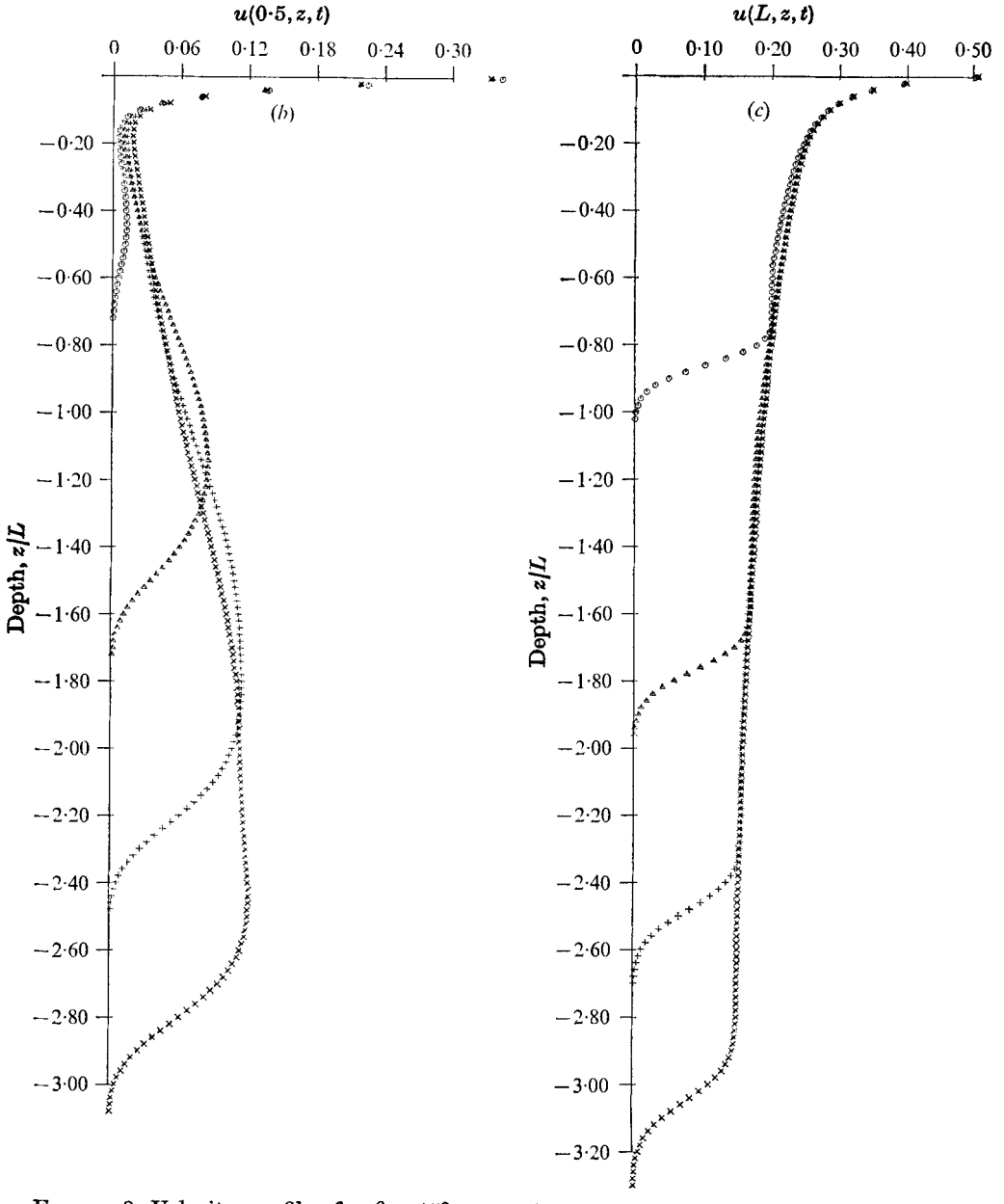

FIGURE 8. Velocity profiles for $\theta = 15°$; note that the velocity scales are not identical. (*a*) At the upwelling cell boundary $y = 0$, (*b*) at a section through the centre of a Langmuir cell $y = \frac{1}{2}L$, (*c*) at the downwelling cell boundary $y = L$. ○, $t = 30{\cdot}34$; △, $t = 60{\cdot}69$; +, $t = 91{\cdot}03$; ×, $t = 121{\cdot}37$. $La = 0{\cdot}01$.

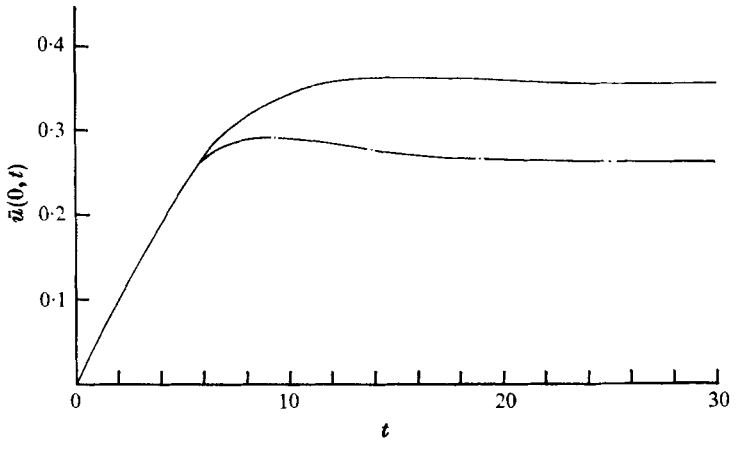

FIGURE 9. Surface current values for the cases in figures 3 and 4. ---, $\theta = 30°$; ——, $\theta = 15°$.

calculations that we have carried out for $\theta = 30°$ used a vertical mesh size of $\Delta z = 0{\cdot}02$ for $0 \leqslant t \leqslant 35$, and then a coarse mesh of $\Delta z = 0{\cdot}1$ was used to continue the calculations beyond $t = 35$. The calculations for $\theta = 15°$ were more time consuming, and the coarse mesh ($\Delta z = 0{\cdot}1$) was therefore used for all calculations shown in figures 4 and 11. The logarithmic region seems to be equally apparent in figure 11, although the small number of points makes its identification less compelling. The inertial sublayers in figures 10 and 11 cover approximately the same depth region, and are about 3 times the thickness of the viscous sublayers. Although this ratio is not large for $La = 0{\cdot}01$, it may be expected to increase as $La \to 0$, since the thickness of the viscous sublayer and La decrease together. In any event, the extent of the inertial sublayer obtained here is not inconsistent with that occurring in low-Reynolds-number turbulent boundary layers (cf. Kline *et al.* 1967, figure 9*a*). The important point to be made is that figure 10 shows that the log region is very *distinct*: each curve is remarkably straight in the interval designated as the inertial sublayer.

The behaviour of the flow below the logarithmic region is complicated, but it appears to be approaching a form analogous to the wake region of the turbulent boundary layer. It should be remembered that all of the profiles shown are instantaneous, and, below the equilibrium zone at least, the flow is developing in time.

Notice that, for each of figures 10 and 11, the slope γ of the inertial sublayer profile is essentially independent of time. Thus, the computations show that the dimensional wind drift current $\overline{U}_c$ (21*a*) in the inertial sublayer is

$$\overline{U}_c = (u_*^2/\nu_T \kappa)\,\overline{u} = (u_*^2/\nu_T \kappa)\,(\overline{u}(0,t) - \gamma \ln (z/z_0)). \tag{46}$$

According to Bye (1965) and to Wu (1975), observed wind drift currents exhibit an inertial sublayer of the form

$$\overline{U}_c = U_{\text{surf}} - (u_*/k) \ln (z/z_0), \tag{47}$$

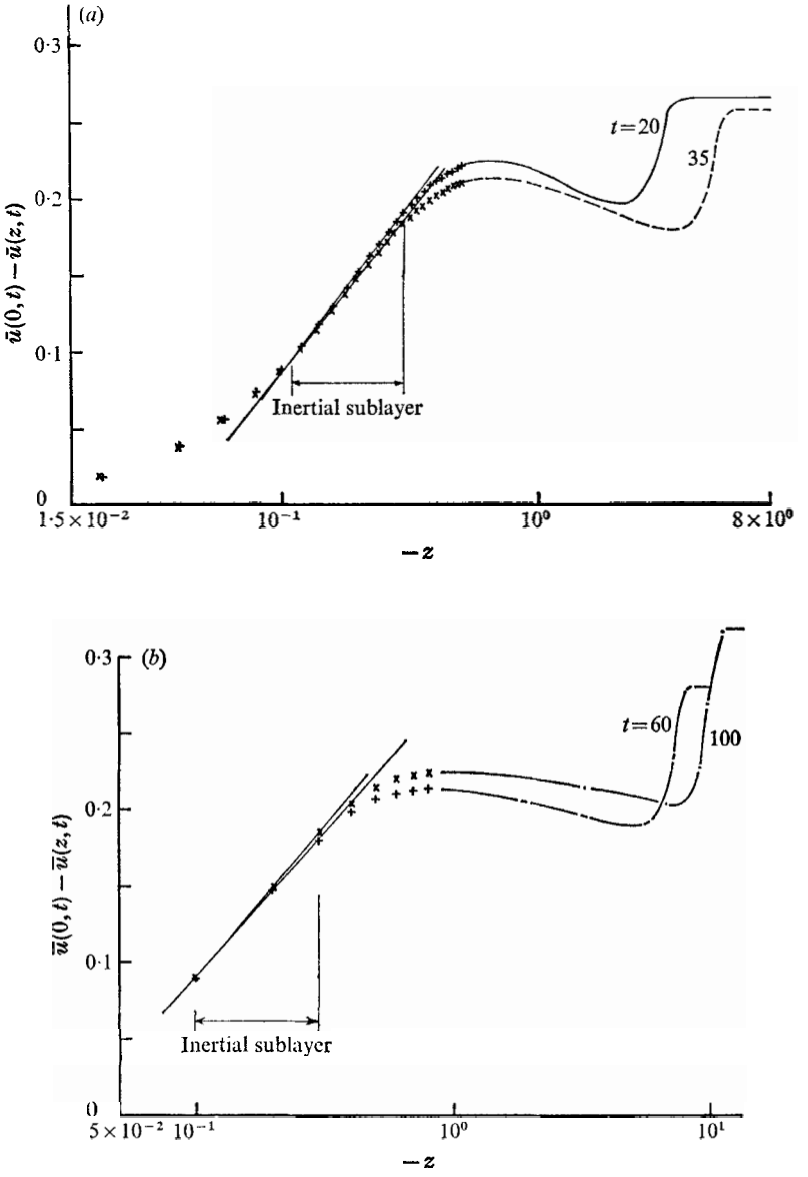

FIGURE 10. (*a*) Two examples of instantaneous velocity-defect profiles plotted on semi-log paper for $\theta = 30°$ and $La = 0{\cdot}01$. The straight line connects points in the inertial sublayer. The computed points in the inertial and viscous sublayers, and a few adjacent points at greater depths are explicitly marked to demonstrate the precision of the straight line fit. $+$, $t = 20$; $\times$, $t = 35$. (*b*) This plot is similar to (*a*), but for larger values of t. A coarse z-mesh was used for these calculations, and therefore the displayed points are more sparse. Nevertheless, the log region remains clear. $+$, $t = 60$; $\times$, $t = 100$. The inertial sublayer for these curves is roughly represented by $\gamma \doteqdot 0{\cdot}087$ in (46).

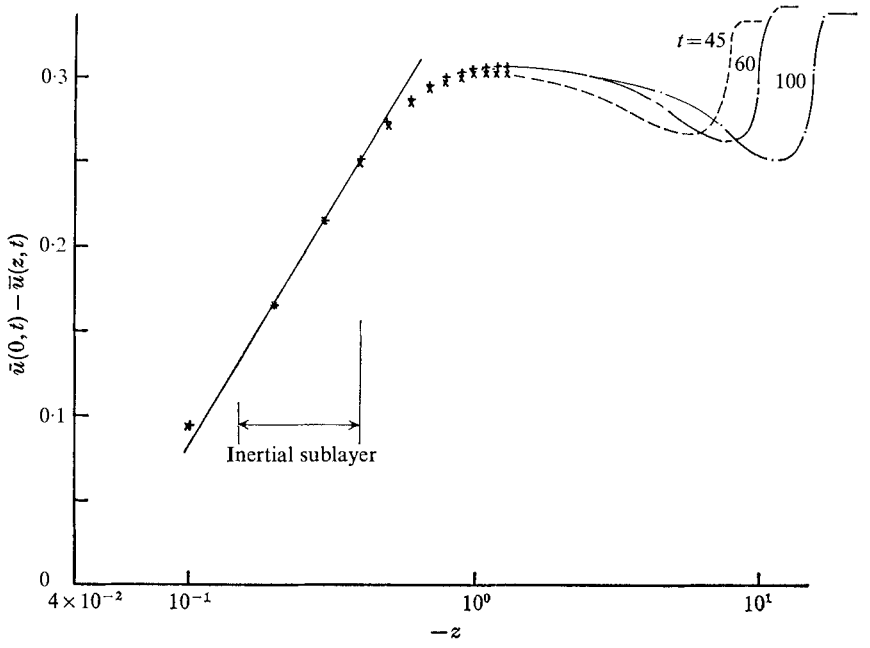

FIGURE 11. The same as figure 10, but for $\theta = 15°$. The point spacing is the same as in figure 10(*b*). Again, the inertial sublayer is distinct. All curves are described reasonably well in the log region by (46) with $\gamma \doteq 0{\cdot}12$.

where $k = 0{\cdot}41$ is von Kármmán's constant and U_{surf} is the surface current speed. Since $\bar{u}(0,t)$ rapidly approaches a constant value (which depends upon θ), U_{surf} might be interpreted as

$$U_{\text{surf}} = (u_*^2/\nu_T\kappa)\,\bar{u}(0,\infty). \tag{48}$$

If we attempt to link the coefficients of the logarithmic terms in (46) and (47), we must suppose that

$$\gamma u_*/\nu_T\kappa = 1/k, \tag{49}$$

so that the surface speed is

$$U_{\text{surf}} = (u_*/k)\,\bar{u}(0,\infty). \tag{50}$$

We shall return to speculations of this sort in the discussion in § 6.

5. Comment on the equilibrium structure in the limit $La \to 0$

Although our problem, as posed, has no steady state, the results that we have presented show that the flow in the equilibrium region approaches a nearly steady state. It would be interesting to determine this quasi-steady motion in the limit $La \to 0$.

The limit problem is singular, and the 'viscous sublayer' must be matched to an inviscid and steady inertial sublayer, which must in turn be matched to an unsteady layer below. We are attempting to carry out this program. At the present time we are in the preliminary stages, and we will only indicate here a simplifying reduction of the equations of the inertial sublayer.

As $La \to 0$, the steady version of (16) is

$$Vu_y + Wu_z = 0, \tag{51}$$

$$V\Omega_y + W\Omega_z = u_z u_{sy} - u_y u_{sz}, \tag{52}$$

$$\nabla^2 \Psi = -\Omega. \tag{53}$$

From (51), $u = \chi(\Psi)$, where χ is an undetermined function of Ψ, and from (52)

$$\begin{aligned} V\Omega_y + W\Omega_z &= \chi'(\Psi)(V\,\partial u_s/\partial y + W\,\partial u_s/\partial z) \\ &= V\partial(\chi' u_s)/\partial y + W\,\partial(\chi' u_s)/\partial z, \end{aligned}$$

which has the solution

$$\Omega = u_s(y,z)\chi'(\Psi) - \Gamma(\Psi).$$

Thus the set (51)–(53) governing the inertial sublayer is equivalent to the single equation

$$\nabla^2 \Psi = \Gamma(\Psi) - u_s(y,z)\chi'(\Psi). \tag{54}$$

The two functions Γ and χ are arbitrary, as far as (51)–(53) are concerned, and must be made definite as part of the matching process. For example, since $u_s \to 0$ exponentially with $-z$, it would appear that $\Gamma(\Psi)$ might be determined by matching vorticity with the unsteady motion at large $-z$. A vorticity match with the viscous sublayer should then determine $\chi'(\Psi)$.

6. Discussion, with emphasis on comparing theory with observation

This paper advances a detailed theory of an extremely complex set of events. We shall now attempt to assess, in a preliminary way, the relation between the theory and nature. The results of this appraisal will prove to be encouraging, but is worthwhile to ask what expectations are reasonable for a detailed description of a geophysical phenomenon. The position taken by Jeffreys (1962) in the preface to his book *The Earth* is worth noting. Jeffreys writes on the question of confirming theoretical models of geophysical phenomena as follows: "... though in some cases formally accurate solutions of related problems exist, or could be obtained, the problems actually so soluble differ so much from those that actually arise in geophysics that, in their actual application, they could at best be correct only as regards order of magnitude" and "a direct proof that a particular hypothesis will account for particular data is not very strong confirmation of the hypothesis when both the data and the consequences of the hypothesis are known only vaguely; but if it is shown that the results of the hypothesis agree with the facts as regards order of magnitude, while the results of denying it are in definite disagreement, the confirmation will be almost as strong as if close agreement had been obtained. The method of exhaustion of alternatives is specially useful in geophysics, because incorrect geophysical hypotheses usually fail by extremely large margins."

While the "consequences of the hypothesis" adopted here have been rather fully explored, the point of view propounded by Jeffreys seems a wise one. We are not in a position presently to make a fully adequate comparison between the results of the present theory and field or laboratory observations, but we can try

to determine if the theory and observation are consistent in the orders of magnitude of the more easily observed quantities. Among these observables are the surface drift speed, the general character of the near-surface motion, particularly the inertial sublayer, and the time scale for current development.

The observed drift of surface water includes the wave drift and the Eulerian drift current $\overline{U}_c$ which we have calculated here, and a proper comparison should include both effects. For now, however, we will neglect the contribution of the wave drift, but keep in mind that it can be comparable to $\overline{U}_c$. The theory of this paper predicts a surface value of $\overline{U}_c$ of

$$U_{\text{surf}} = (u_*^2/\nu_T \kappa)\,\overline{u}(0,\infty).$$

The parameters ν_T and κ are not easily determined. From § 5, however, the near-surface motion in the inertial sublayer in theory and observation can be made to agree if (49) holds. This implies that

$$U_{\text{surf}} = (u_*/k\gamma)\,\overline{u}(0,\infty),$$

so that the surface drift speed is proportional to the friction velocity. The air friction velocity can be estimated to be between $\frac{1}{22}$ and $\frac{1}{25}$ of the wind speed, and the water friction can be estimated by equating the wind and water stress. This procedure (which ignores that proportion of the wind stress supported by wave drag) yields

$$(u_*)_a/(u_*)_w = (\rho_w/\rho_a)^{\frac{1}{2}} \approx 30, \tag{55}$$

where the subscripts a and w stand for air and water. This estimate is consistent with the data reported in figures 2 and 9 of Wu's (1975) paper. Laboratory and field studies indicate that the wind drift is directly proportional to (typically 3 to 4 % of) the wind speed, and therefore indirectly to the water friction velocity. Also, according to Wu, and to Phillips & Banner (1974), the surface current speed is about $0{\cdot}55(u_*)_a$. Using the relation between $(u_*)_a$ and $(u_*)_w$ presented above, the surface speeds are $16{\cdot}5(u_*)_w$. Both of the finite-difference solutions that have been described in this paper produce values of $\overline{u}(0,\infty)$ and γ of $0{\cdot}3$ and $0{\cdot}1$ (when rounded to one significant figure). (Both $\overline{u}(0,\infty)$ and γ appear to depend upon the parameters θ and La, although our calculations are not adequate to determine the dependence.) If we adopt these values and insert $k = 0{\cdot}4$ for von Kármán's constant, our calculations yield a frictional surface wind drift

$$U_{\text{surf}} = u_* \overline{u}(0,\infty)/\gamma k \approx 7{\cdot}5 u_*,$$

which is about half of the value observed for the frictional and wave drift currents combined. Smaller values of θ should lead to increased $\overline{u}(0,\infty)$, however, since mixing reduces surface current speeds and the effects of mixing are reduced as θ decreases. The relative magnitudes of the wave drift and the friction current are only poorly understood, and we do not have a definite principle to select a value for θ in our model. Consequently, we think that the above comparison of U_{surf} with observation, being reasonable in numerical order of magnitude, is encouraging.

The time scale for the development of the current (designated as T_d) is, according to (19a),

$$T_d \equiv \sigma^{-1}(\nu_T \sigma)^{\frac{1}{2}}/\epsilon u_*.$$

The numerical calculations show (figure 9) that the surface current is essentially fully developed in a dimensionless time of under 10 units, so the time scale assumed in the theory is an appropriate one for the surface current. We shall attempt to estimate this time scale by adopting (49) to eliminate the most awkward term, ν_T. This yields

$$T_d = \epsilon^{-1}(k\gamma c/u_*)^{\frac{1}{2}}\sigma^{-1},$$

where c is the wave phase speed σ/κ. A crude estimate of this can be arrived at by adopting $\gamma = 0{\cdot}1$, by setting c equal to the wind speed, which is assumed to equal $22(u_*)_a$, and by adopting (55). With these steps taken,

$$T_d \sim 5\epsilon^{-1}\sigma^{-1}.$$

In the formulation used in this paper $2\epsilon\cos\theta/\pi$ is a measure of the wave slope (see § 3). For a wave slope of $\frac{1}{10}$ and small θ, $\epsilon \sim 0{\cdot}15$, and

$$T_d \sim 33\sigma^{-1}.$$

Since σ^{-1} is generally of the order of seconds, T_d is of the order of minutes.

The range of interest for La can be estimated if we again use (49) to eliminate ν_T; this yields

$$La = (k\gamma)^{\frac{3}{2}}(u_*/c)^{\frac{1}{2}}/\epsilon.$$

Using the values of ϵ and γ, and the replacement for c used in the estimate for T_d, we arrive at $La \sim 0{\cdot}002$. The precise value is not of importance, but it is of interest to know that La is small, for in our model small La indicates that the momentum transfer by the organized convective motions dominates that accomplished by the small-scale turbulent motions.

7. Conclusion

A comprehensive theoretical model has been presented for Langmuir circulations and the horizontally averaged frictional wind drift currents in the ocean. On the basis of arguments made previously by Craik & Leibovich, the model postulates that the Langmuir circulations and the wind drift are interconnected and form parts of an inseparable current system.

Three assumptions are fundamental to the theory: (i) that surface waves can, because of their directional propagation characteristics, produce a wave drift in the wind direction that oscillates in magnitude across the wind; (ii) that the wave orbital speeds are much larger than the frictional drift that develops; and (iii) that the time scale for the development of the current is large compared with a wave period, so that a multiple-time-scale analysis can be applied. Granted these assumptions, the model is constructed from first principles. Other assumptions are made to simplify the analysis, but do not appear to be essential to the theory.

Despite the simplifications required to make the mathematics tractable, the predictions of the model agree well with experimental findings on the wind drift current. In particular, the current profiles are similar in form and the magnitudes of the currents are in acceptable agreement. More important, the scalings that

emerge from the model are internally consistent when semi-empirical correlations are used to estimate the input parameters.

We note, finally, that it seems possible to incorporate into the model slow changes in the wave parameters and in the wind stress. All that seems to be required is that these parameters should not vary rapidly compared with the time scale T_d for development of the wind drift current and Langmuir circulations.

This paper has been materially improved by the incorporation of helpful comments on earlier versions of the work by several people. Remarks by Professor G. O. Roberts and a session with Professors S. Corrsin, S. H. Davis and O. M. Phillips were particularly valuable. Questions raised by Dr A. D. D. Craik have led to clarification of the text on a number of important points. I would like also to acknowledge, with gratitude, the support provided by the National Science Foundation under Grants GA-43241 and DES74-13057A01.

Appendix

The functions f_1 and f_2 defined in (36) and (40) were constructed directly from the integral formulae (42) and (45). The functions ϕ_m and θ_m satisfy (44), and the relations

$$g'_{m+1}(\tilde{\eta}) = g_m(\tilde{\eta}), \tag{A 1}$$

$$mg_m(\tilde{\eta}) = \tilde{\eta} g_{m-1}(\tilde{\eta}) + \tfrac{1}{2} g_{m-2}(\tilde{\eta}). \tag{A 2}$$

The recursion relation (A 2) was used to evaluate ϕ_m and θ_m numerically. The ϕ_m family was found by selecting the starting solutions $\phi_{-1} = 0$, $\phi_0(\tilde{\eta}) = 1$, and the θ_m family was found by starting with

$$\theta_{-1}(\tilde{\eta}) = 2\pi^{-\frac{1}{2}} \exp(-\eta^2), \quad \theta_0(\tilde{\eta}) = \operatorname{erfc}(-\tilde{\eta}).$$

It can be seen that for all integers n,

$$\phi_{2n+1}(0) = 0,$$

$$\theta_{2n+1}(0) = [2^n(2n+1)(2n-1)\ldots 5.3.1.\sqrt{\pi}]^{-1},$$

while

$$\phi_{2n}(0) = \theta_{2n}(0) = (2^{2n} n!)^{-1}.$$

Provided the functions R_1 and R_3 in (42) and (45) do not grow as $\tilde{\eta} \to -\infty$, all integrals in (42) and (45) converge.

In the integration by parts used in going from (43) to (45), use has been made of the formula

$$d(\exp(\nu^2) g_m(\nu))/d\nu = 2(m+1) \exp(\nu^2) g_{m+1}(\nu)$$

that is satisfied (in view of (44) and A 1) by the g_m.

With ϕ_m and θ_m evaluated as described above, the integrals in (42) and (45) were evaluated using the subroutine DQSF described in the IBM Scientific Subroutine Package, using a step size of 0·05. Accuracy was assessed by repeating the calculation with the mesh reduced to 0·025. The computer program was also verified, and its accuracy determined, by calculating both (42) and (45) for examples of R_1 and R_3 that yield exactly known solutions. In the case of (42), the

solution when $R_1 = -14\exp(\tilde{\eta}^2)$ is $\exp(-\tilde{\eta}^2)$. Also, $\exp(-\tilde{\eta}^2)$ is the proper solution to (45) if $R_2 = -12\sqrt{\pi}\,\mathrm{erfc}(-\tilde{\eta})$. The exact solutions were reproduced by the program to four significant figures with a step size of 0·05.

REFERENCES

BENNEY, D. J. & LIN, C. C. 1960 On the secondary motion induced by oscillations in a shear flow. *Phys. Fluids*, **3**, 656–657.

BYE, J. A. T. 1965 Wind-driven circulation in unstratified lakes. *Limnol. Oceanogr.* **10**, 451–458.

CRAIK, A. D. D. & LEIBOVICH, S. 1976 A rational model for Langmuir circulations. *J. Fluid Mech.* **73**, 401–426.

FALLER, A. J. 1971 Oceanic turbulence and the Langmuir circulations. *Ann. Rev. Ecology & Systematics*, **2**, 201–236.

GORDON, A. L. 1970 Vertical momentum flux accomplished by Langmuir circulations. *J. Geophys. Res.* **75**, 4177–4179.

JEFFREYS, H. 1962 *The Earth*, 4th edn. Cambridge University Press.

KLINE, S. J., REYNOLDS, W. C., SCHRAUB, F. A. & RUNSTADLER, P. W. 1967 The structure of turbulent boundary layers. *J. Fluid Mech.* **30**, 741–774.

LEIBOVICH, S. & RADHAKRISHNAN, K. 1977 On the evolution of the system of wind drift currents and Langmuir circulations in the ocean. Part 2. Numerical solutions for the Langmuir cells. *J. Fluid Mech.* (in press).

LEIBOVICH, S. & ULRICH, D. 1972 A note on the growth of small scale Langmuir circulations. *J. Geophys. Res.* **77**, 1683–1688.

LONGUET-HIGGINS, M. S. 1953 Mass transport in water waves. *Phil. Trans.* A **245**, 535–81.

PHILLIPS, O. M. 1966 *Dynamics of the Upper Ocean.* Cambridge University Press.

PHILLIPS, O. M. & BANNER, M. L. 1974 Wave breaking in the presence of wind drift and swell. *J. Fluid Mech.* **66**, 625–640.

ROACHE, P. J. 1972 *Computational Fluid Dynamics.* Albuquerque: Hermosa Publishers.

SCOTT, J. T., MYER, G. E., STEWART, R. & WALTHER, E. G. 1969 On the mechanism of Langmuir circulations and their role in epilimnion mixing. *Limnol. Oceanogr.* **14**, 493–503.

SHEMDIN, O. H. 1972 Wind-generated current and phase speed of wind waves. *J. Phys. Ocean.* **2**, 411–419.

STEWART, R. W. 1967 Mechanics of the air–sea interface. *Phys. Fluids Suppl.* **10**, S47–55.

WU, J. 1969 An estimation of wind effects on dispersion in wide channels. *Water Resources Res.* **5**, 1097–1104.

WU, J. 1975 Wind-induced drift currents. *J. Fluid Mech.* **68**, 49–70.